JOURNAL OF MATERIALS SCIENCE 26 (1991) 1609 - 1617

Interface and fracture of carbon fibre reinforced Al–7 wt % Si alloy

M. YANG, V. D. SCOTT
School of Materials Science, Bath University, Bath, UK

The interface structure in an aluminium–7 wt % silicon alloy reinforced with carbon fibres has been investigated using analytical electron microscopy. Crystals of aluminium carbide (Al_4C_3) have been identified in interface regions and their structure and growth are discussed. Mechanical properties of the composite have been measured and fracture behaviour studied using acoustic emission analysis in parallel with microstructural examination. The results indicated that the aluminium carbide interfacial reaction had produced a strong fibre matrix bond, but reduced the fibre strength and embrittled the matrix. Consequently, whole fibre bundles failed in a brittle manner in the longitudinal direction with limited pull-out of individual fibres. The findings are discussed in relation to the method used to manufacture the composite.

1. Introduction

The demand for lightweight materials having improved specific strength and stiffness has generated considerable interest in the development of aluminium alloy composites reinforced with high strength, low cost carbon fibres [1, 2]. One technique for the production of such composites involves molten metal infiltration of fibre preforms with the aid of external pressure [3], its attraction being a capability to produce net shaped, complex engineering components with high efficiency. The method has problems, however, due to the possibility of a chemical reaction occurring between reinforcement and matrix at the infiltration temperature. Indeed, if such a reaction does take place the likely loss of fibre strength and local embrittlement of the matrix would result in a lower failure strain and fracture toughness of the composite.

Although the reaction between carbon and aluminium has been studied by several authors, there is only limited published information concerning the crystallography and morphology of aluminium carbide and, when present in a composite, its effect on mechanical properties. In the case of transmission electron microscopic studies, the technical difficulties of preparing reliable thin specimens from a material containing water soluble compounds, and of analysing areas of interest typically much smaller than 0.5 μm may be contributory factors.

Khan [4] studied diffusion couples prepared by depositing films of aluminium onto carbon substrates and reported that an approximately 4 μm thick layer of carbide formed at the interface after heat treatment of the specimen at 600 °C for 24 h. He stated that the carbide grew as single-crystal platelets perpendicular to the *c* axis of the lattice, although no details were presented to support the conclusion. An alternative approach involving aluminium deposited onto carbon fibres was adopted by Baker and Bonfield [5]. They reported aluminium carbide formation after annealing coated fibres for 100 h at temperatures above 475 °C and related the microstructural change with a degradation in fibre strength. A similar experiment by Okura and Motoki [6] appeared to confirm aluminium carbide formation although they quoted a much lower rate of carbide growth than Khan, a 70 nm thick layer of carbide being formed after treatment for 24 h at 600 °C. These apparently conflicting data may be attributed to some extent to the effect of oxide layers on the wetting of molten aluminium [7] or to the different degrees of graphitization of the carbon samples, and further work is clearly needed to help resolve the matter.

In the present paper, the microstructure of the fibre–matrix interface in an Al–7 wt % Si alloy composite reinforced with carbon fibres is studied using a range of techniques including optical and analytical electron microscopy. In parallel, mechanical properties of the composite are investigated using four-point bend tests coupled with acoustic emission analysis. Fracture behaviour is analysed on the basis of microstructural data and acoustic characteristics, and the role of the fibre–matrix interface with respect to the mechanical behaviour of the composite is discussed.

2. Experimental procedure

The composite material studied was an aluminium–7 wt % silicon–0.2 wt % magnesium alloy reinforced with PAN-based low modulus carbon fibres*. Nominal properties of the fibre were: tensile strength 3.4 GPa, tensile modulus 230 GPa, failure

*Courtaulds XA HP, Courtaulds Ltd.

0022–2461/91 $03.00 + .12

strain 1.5% and density 1.80 g cm^{-3}. They were supplied as 10 000 multiply tows interwoven with glass fibre wefts and were unidirectionally aligned in the metal matrix. The composite was manufactured using liquid metal infiltration [3] of the fibre preform at an applied pressure of less than 7 MPa and melt temperature of $\sim$ 750 °C. A sample of the unreinforced alloy was included for comparison purposes.

Strength tests were performed using the four-point bending mode on an Instron machine at a cross-head speed of 0.5 mm min^{-1}. Nominal dimensions of the specimen were 70 × 10 × 5 mm^3. A strain gauge glued on the tensile surface of the specimen measured deformation and a Dunegan acoustic emission transducer monitored acoustic signals generated during the test.

Polished sections and fracture surfaces of composite were examined with a Zeiss ICM 405 optical microscope and also with a JEOL 35C scanning electron microscope (SEM) equipped with a LINK AN10000 energy dispersive spectrometer (EDS).

Specimens for TEM studies were prepared by slicing thin 3 mm diameter discs in directions parallel and transverse to the fibre. Discs were dimpled on both sides using a VCR model D500 and then ion milled in a Gatan Duomill 600; a voltage of 5 kV and an incidence beam angle of 15° was used until perforation and then a voltage of 3 kV and an incidence beam angle of 10° to increase the area of sample transparent to the electron beam. Thinned specimens were examined in a JEOL 2000FX microscope fitted with a LINK 10000 EDS system and a thin window, high take-off angle detector for improved light element performance.

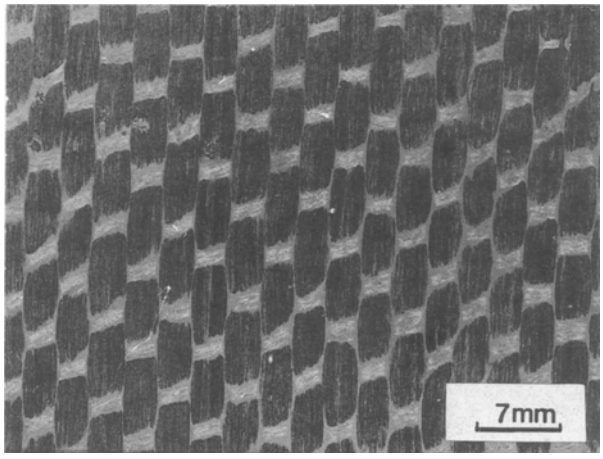

Figure 1 Carbon fibre reinforced Al–7 wt % Si alloy; each division is 1 mm, OM.

3. Results

3.1. Optical and scanning electron microscopy

Fig. 1 shows the as-received composite. The carbon fibre tows appear as dark bands, with the glass fibre wefts used to fix the tows visible as light grey constituents aligned approximately at right angles to the carbon fibres. A transverse section of the composite, Fig. 2, shows a uniform distribution of fibres in the tow and little visible porosity at this magnification. Close fibre packing near the edge of the tow is evidence of fibres being forced together by the pressure of the liquid metal infiltration front. White particles may be seen adjacent to fibres, which EDS analysis indicated contained some iron presumably introduced as contaminant during infiltration [8]. Image analysis using a Magiscan system showed that the packing density of fibres in the tow was approximately 65 vol % and that the total volume fraction of carbon fibres in the composite was 48 vol %; glass fibres amounted to some 5 vol % of the total bulk. The aluminium–silicon eutectic structure which characterizes this alloy is not clearly visible in the above picture but Fig. 3 shows its distribution in matrix regions between the fibre tows; where the interfibre spacing is small the silicon particles tend to form interfibre bridges.

3.2. Analytical transmission electron microscopy

Fig. 4a illustrates an interfacial region between a carbon fibre and the aluminium alloy matrix. A reaction zone is evident which contains lath-like crystals of width $\sim$ 20 nm and length up to 500 nm. The crystals

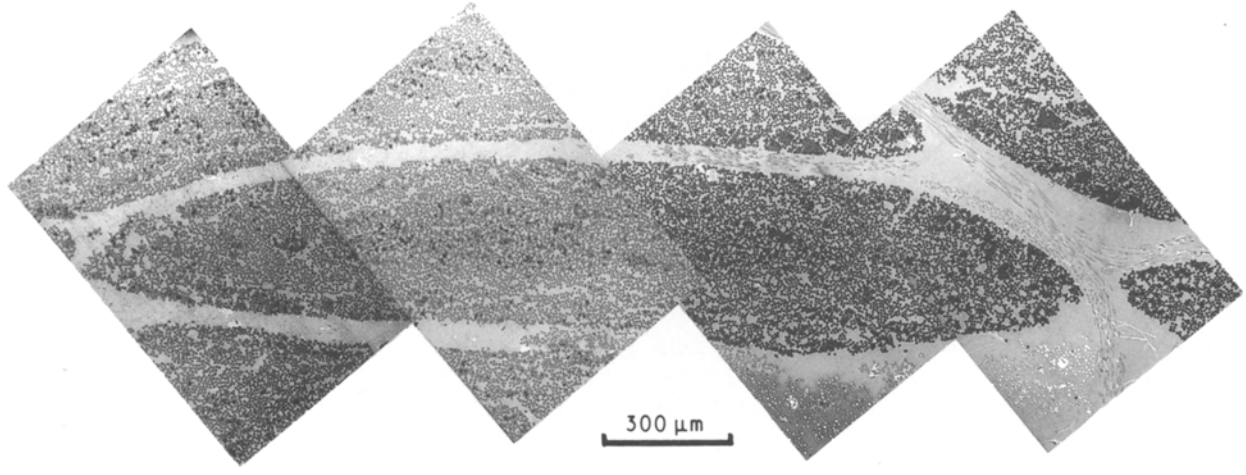

Figure 2 Section through composite showing discrete fibre tow, OM.

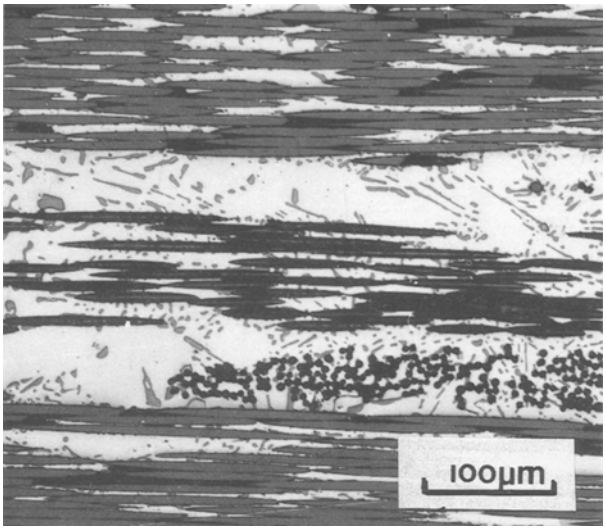

Figure 3 Composite showing aluminium–silicon eutectic structure of matrix, OM.

carbon was presumably a contaminant transported from neighbouring carbon fibres during specimen preparation, whilst the oxygen was due to surface oxidation of the aluminium foil. The EDS spectrum from the interfacial region Fig. 4c, shows substantial aluminium and carbon with a small amount of oxygen. It is not clear whether in this case the oxygen is part of the fibre–matrix interfacial structure of the composite, as has been suggested by Everett *et al.* [10] or whether it is a surface artefact as in Fig. 4b.

A lattice image taken from a lath-like crystal, Fig. 5a, reveals fringes with a spacing of 0.84 nm lying parallel to the axis; note the steps along the edge of the crystal. An EDS spectrum from the crystal, Fig. 5b, obtained with an electron probe diameter of less than 20 nm, shows that it consists only of aluminium and carbon, indicative of aluminium carbide. Microbeam diffraction, Fig. 5c, reveals that the carbide crystal has rhombohedral symmetry with a space group R3m and

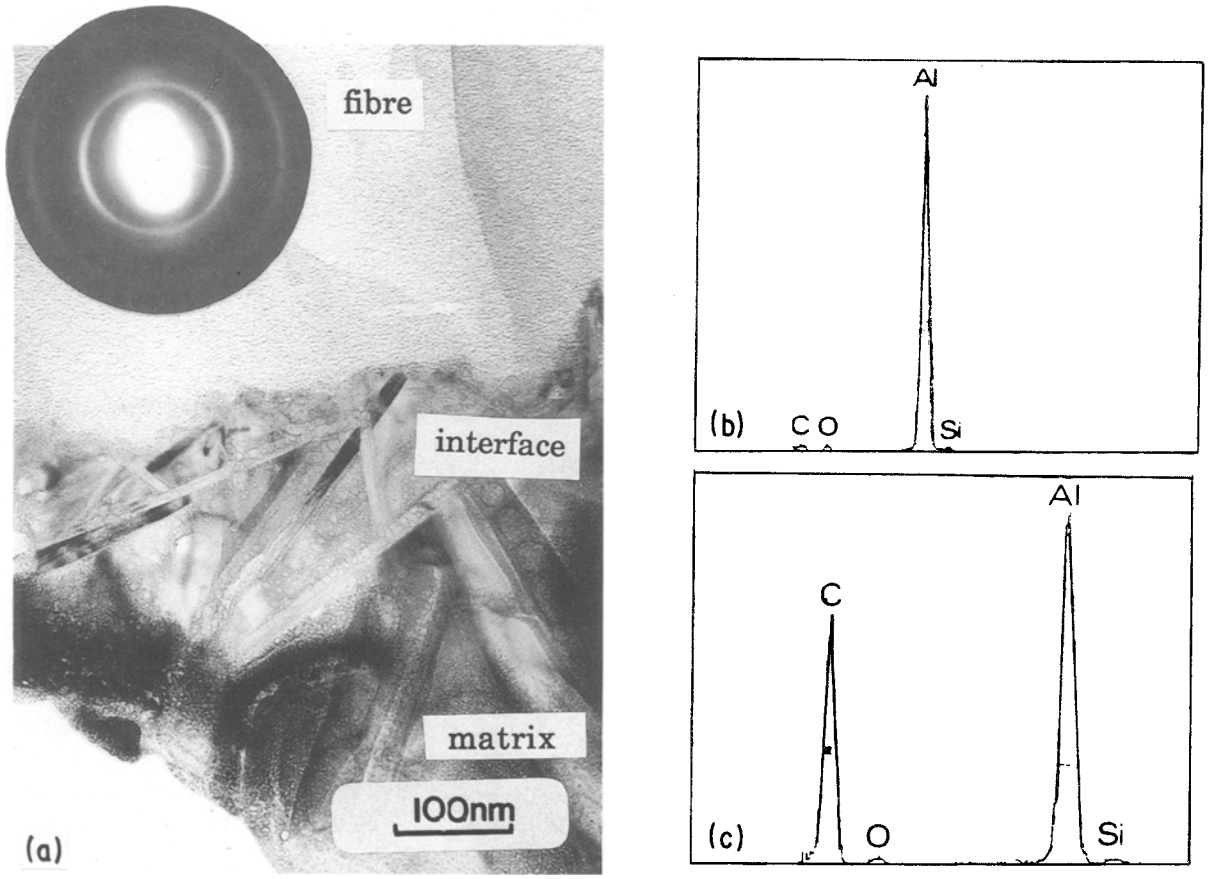

Figure 4 Fibre–aluminium interface, (a) TEM, (b) EDS spectrum from matrix, (c) EDS spectrum from interface.

appear to nucleate in the vicinity of the fibre and then to grow into the matrix in a variety of directions. Diffraction analysis, Fig. 4b, indicates that the basal planes of the carbon lattice are approximately aligned ($\pm$ 15°) along the axis of the fibre and are oriented randomly around this direction. Analysis of the matrix using EDS, Fig. 4b, shows it contains small amounts of silicon, carbon and oxygen. The silicon content accords with the amount expected in solution in aluminium at the temperature of infiltration [9], the lattice parameters $a = 0.334$ nm and $c = 2.5$ nm. The row of strong reflections are 0003, 0006 and 0009, the most intense reflection 000, 12 corresponding to the number of basal layers in the unit cell of aluminium carbide [11]. Parallel rows of $1\,1\,\bar{2}l$ and $\bar{1}\,\bar{1}\,2l$ spots were visible in the negative but have not reproduced well in the print. The lattice fringes seen in Fig. 5a thus correspond to the basal planes of the carbide lattice, three fringe spacings of 0.84 nm equating with its c axis dimension. Furthermore, the longi-

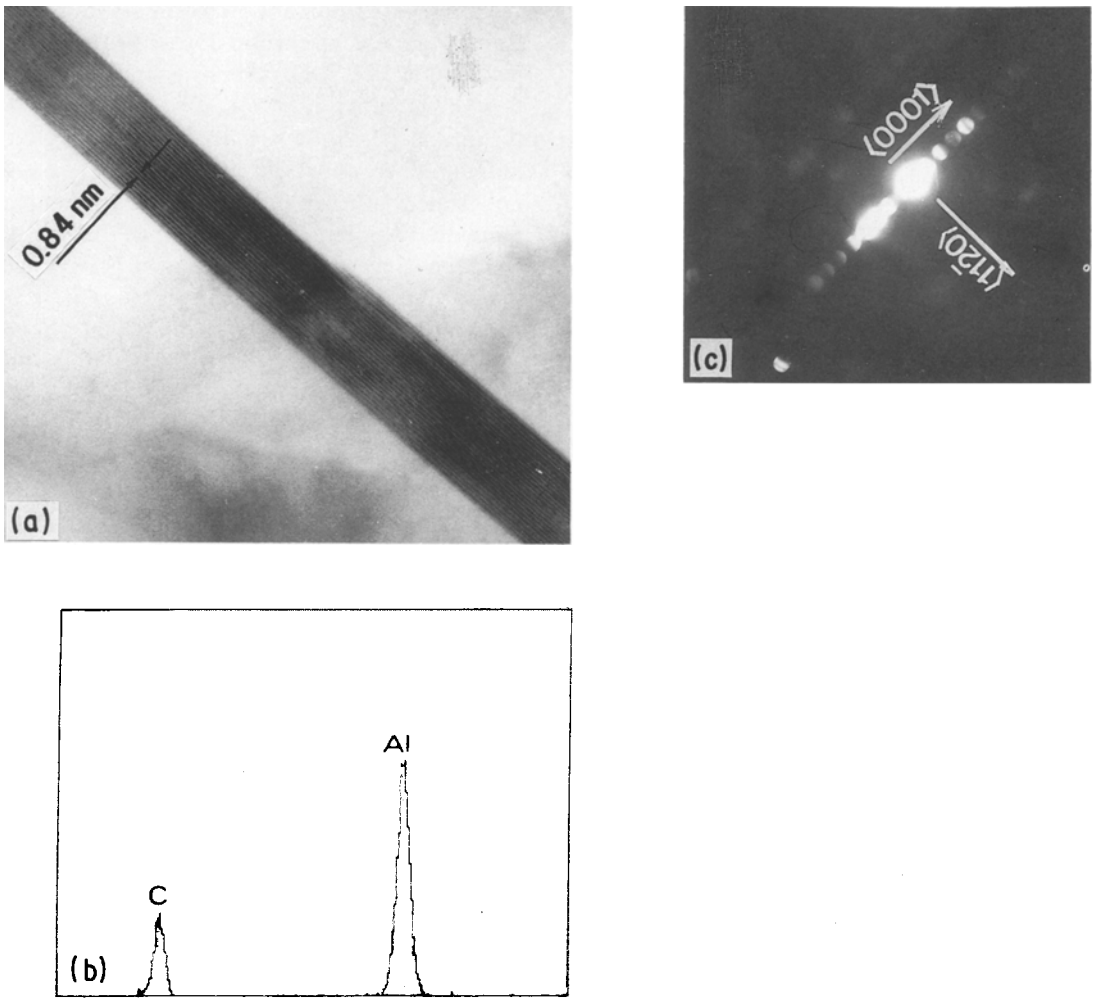

Figure 5 Carbide crystal in matrix, (a) TEM showing lattice fringes, (b) EDS spectrum from crystal, (c) SAD from crystal.

tudinal axis of the crystal is closely parallel to the carbide [1 1 $\bar{2}$ 0] direction. All carbide crystals which were analysed were found to have basal planes oriented parallel to the longitudinal axis. Where carbon fibres were relatively close together, the carbide crystals sometimes formed a "bridge" between them.

The fibre–matrix interface structure was quite different where a particle of the matrix silicon contacted the fibre, Fig. 6a, the interface being well defined with no evidence of any chemical reaction having taken place. This observation accords with published chemical data on aluminium and silicon interactions as they relate to the liquid metal infiltration temperature of around 750 °C [12]. Analysis of a selected area diffraction (SAD) pattern from the silicon, Fig. 6b, showed that the parallel lamellae of differing contrast were twins. The other end of the twinned silicon appeared also to make contact with a carbon fibre, Fig. 7, but here crystals identified by EDS and SAD as the aluminium carbide, were present. The difference between the two interface structures is most likely a result of the metal solidification sequence. It is envisaged that the silicon particle first solidified on the fibre illustrated in Fig. 6a, and then grew towards the other fibre during the course of further solidification. By the time it reached the second fibre interface, however, chemical reaction of the fibre with aluminium had already taken place, Fig. 7, to form carbide crystals of the type illustrated and identified in Fig. 5a to b.

Dislocations were a common feature of the aluminium matrix adjacent to fibres as would be expected from the differential thermal contraction of the two components. Fig. 8 shows an array of dislocations which appear to be initiated from the fibre–matrix interface and to be moving away. It may be seen that the dislocation density decreased with distance from the interface. Assuming a foil thickness of 150 nm in this region gives a dislocation density of $\sim 2 \times 10^8\ mm^{-2}$, a figure which is typical of aluminium subjected to $\sim 1\%$ cold work. For this composite system, a thermal strain of 1.5% would be predicted upon cooling from the infiltration temperature, taking thermal expansion coefficients of $-1.0 \times 10^{-6}\,°C^{-1}$ and $23 \times 10^{-6}\,°C^{-1}$ for fibre and matrix respectively [13]. This value is sufficient to cause matrix yielding and to produce an internal stress which accords with the observed dislocation density.

3.3. Mechanical behaviour

Typical stress against strain curves, obtained in four-point bend tests on longitudinal and transverse specimens, are plotted in Fig. 9; the data were obtained from a strain gauge affixed to the tensile surface.

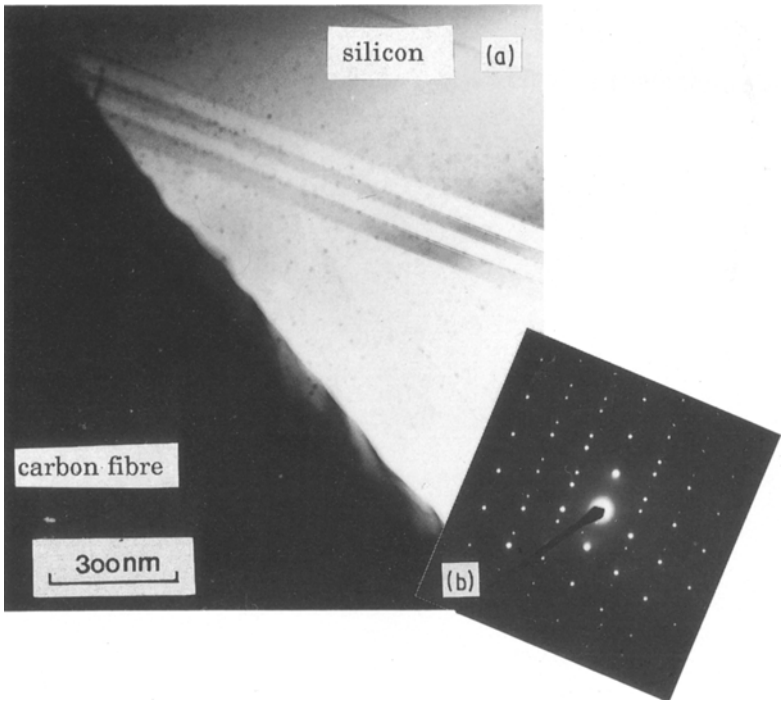

Figure 6 Fibre–silicon interface: (a) TEM showing twinned silicon crystal, (b) SAD from twinned silicon crystal.

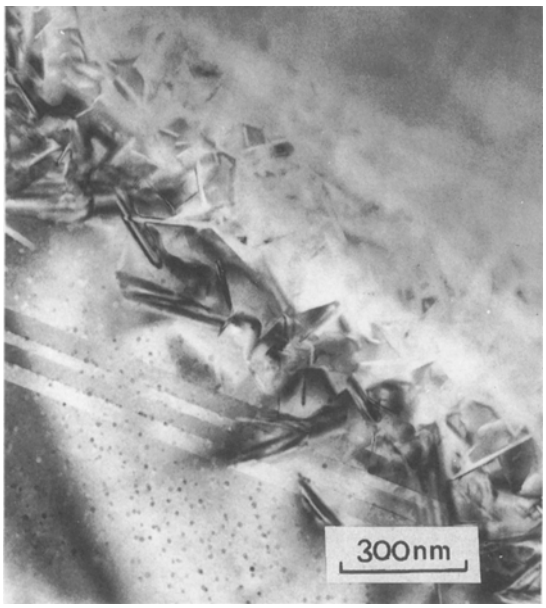

Figure 7 Fibre–silicon interface; TEM showing twinned silicon and carbide crystals.

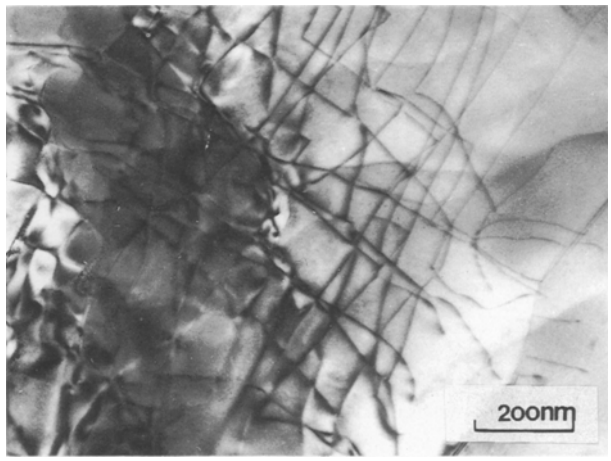

Figure 8 Region near fibre–aluminium interface showing dislocations, TEM.

Results for the unreinforced alloy are also included in the diagram.

The unreinforced alloy deformed elastically up to a stress of about 50 MPa, to give a yield stress of 75 MPa at a proof strain of 0.2%. The test was terminated before the material fractured because of the limited extension range of the strain gauge. Young's modulus of the alloy calculated from the initial linear section of the stress against strain curve was 64 GPa.

The test of the longitudinal composite resulted in a linear stress against strain curve up to about 120 MPa, beyond which it showed a slight deviation from linearity. Sudden failure occurred at 256 MPa with an accompanying strain of 0.20%. The tensile modulus of the composite deduced from the initial linear regime was 160 GPa. The average strength of the composite determined from five tests was 285 MPa and the mean failure strain was 0.22%. Acoustic emission data, Fig. 10, were characterized by a quiet period until the failure stress was reached, whereupon the event rate increased sharply. This coincided with gross fracture of fibre bundles.

The microstructure of the longitudinal specimen showed brittle fracture of fibre bundles and some plastic necking of the matrix, as seen in Fig. 11a taken from the tensile surface of the specimen close to the fracture. A second feature, presented in Fig. 11b, shows multiple fibre fracture with cracks propagating across fibre bundles in a straight fashion when individual fibres are closely spaced. Where, however, there is a substantial amount of matrix material, the crack is seen to be arrested. The fracture surface, Fig. 12a, had

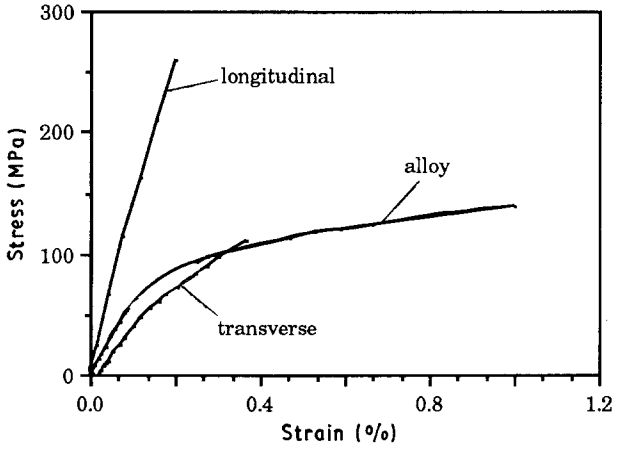

Figure 9 Stress against strain curves from tensile tests.

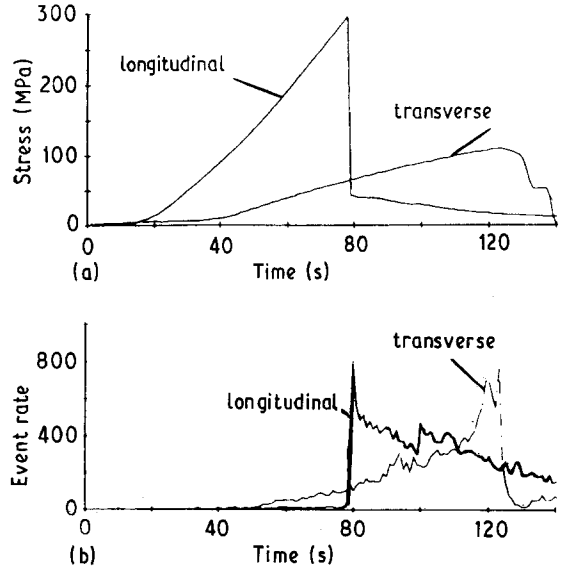

Figure 10 Acoustic emission from four-point bend tests, (a) stress against time, (b) event rate against time.

a flat appearance with little fibre pullout and this seemed to take place in regions where fibres were closely packed and poorly infiltrated. Fig. 12b shows longitudinal porosity in interstices between fibres and a smooth and flat fracture surface to the carbon fibres. The matrix was also smooth in the proximity of fibres (~ 2 μm), a feature which extended well beyond the carbide reaction zone (width ~ 0.5 μm). Further away from the fibres, however, plastic deformation of the matrix was evident.

In the test of the transverse specimen, the stress–strain curve of the composite exhibited a less extensive linear relationship and showed appreciable plastic deformation. Failure occurred at 108 MPa with an associated strain of 0.39%. The tensile modulus was estimated from the initial part of the stress against strain curve as ~ 40 GPa. The average strength determined from five tests was 102 MPa with the mean failure strain of 0.36%. Acoustic emission, Fig. 10, commenced at a stress close to the matrix yield stress of ~ 50 MPa and increased progressively with the degree of plastic deformation. Intermittent

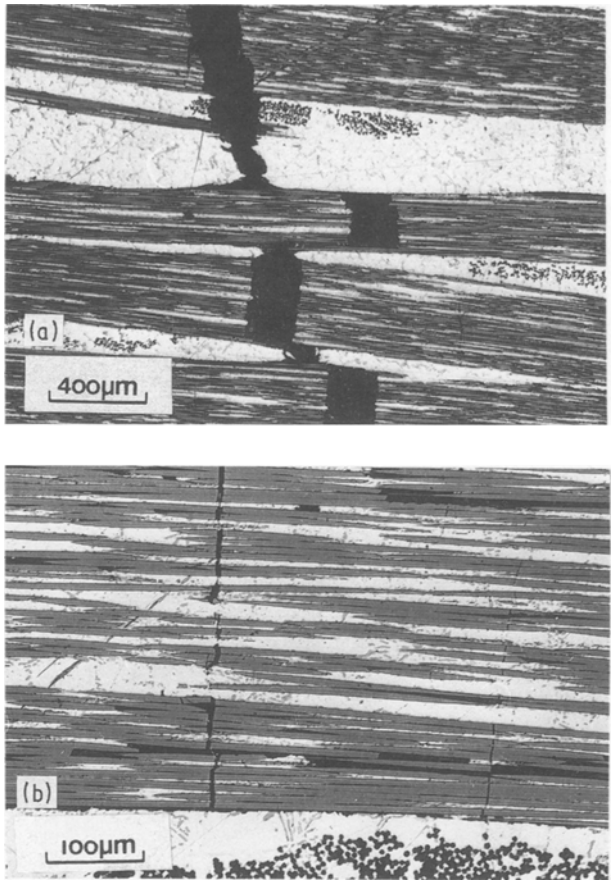

Figure 11 Tensile tested longitudinal specimen, polished section showing (a) fracture of fibre bundles, (b) crack arrest at large matrix region, SEM.

increases in event rate are possibly related to the consecutive fracturing of glass fibres.

The fracture surface of a transverse specimen is illustrated in Fig. 13a, an area which includes most of a carbon fibre tow plus some glass fibre weft. The weft fibres aligned perpendicularly to the fracture surface have broken in a brittle manner. Carbon fibres at the edge of the tow (close to the glass wefts) have a clean surface, indicative of cracks by-passing interfacial porosity, but fibre splitting along the axis can be seen in the middle of the tow, Fig. 13b. Exposed fibre surfaces have a pitted appearance confirming the presence of some interfacial reaction. A section through a transverse specimen taken from the tensile surface near the major crack is illustrated in Fig. 14. Note the tendency for the crack to propagate around a fibre tow in regions of close fibre packing where, as shown in Fig. 12b, longitudinal porosity was present. Some limited plastic deformation of the metal matrix is apparent.

4. Discussion

4.1. Interfacial structure

The present results show clearly that a chemical reaction between aluminium and the carbon fibres has taken place during the liquid metal infiltration process. No reaction between the silicon constituent of the matrix and a fibre was, however, observed. The reaction product has been confirmed as rhombohedral

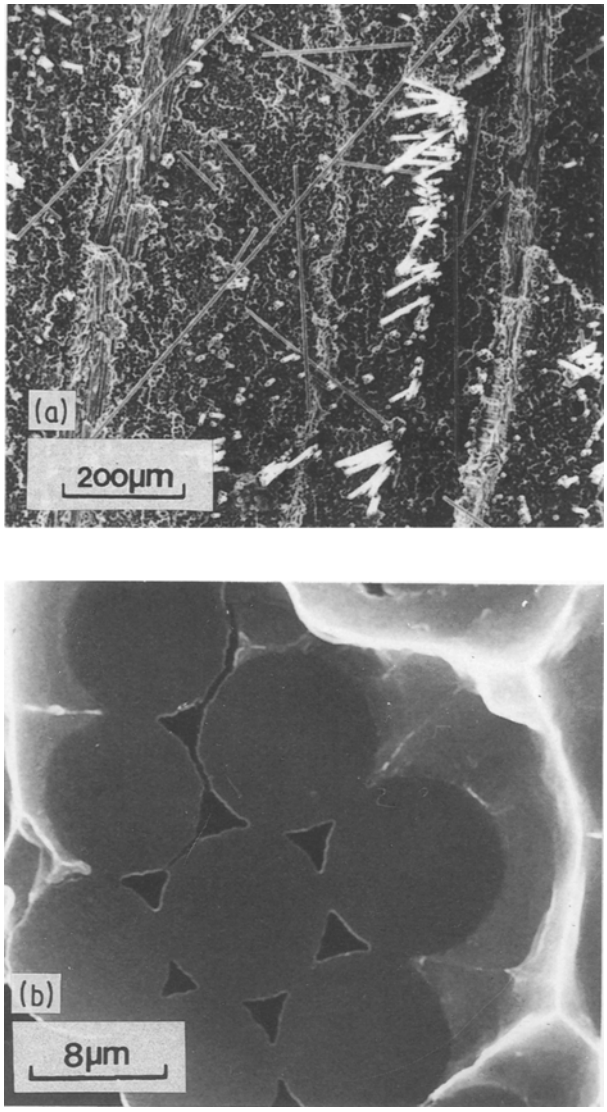

Figure 12 Tensile tested longitudinal specimen; fracture surface showing (a) flat surface (b) close fibre packing, SEM.

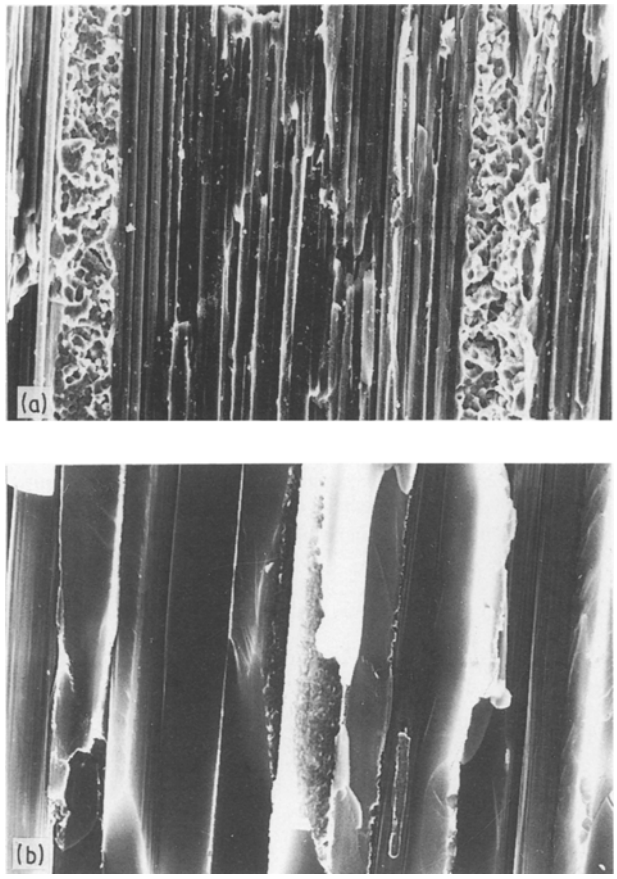

Figure 13 Tensile tested transverse specimen; fracture surface of (a) an entire tow (b) middle of tow showing fibre splitting, SEM.

aluminium carbide of the type Al_4C_3. The carbide has been observed to nucleate heterogeneously from the fibre and to grow into the aluminium matrix as lath-like crystals of width less than 20 nm and an aspect ratio of up to 30. The axis of the crystal lies parallel to the basal plane of the crystal lattice. These observations lead to the following conclusions.

(a) Nucleation of the carbide is associated with defects present on the surface of the carbon fibre such as exposed basal plane edges. The spread in orientation of basal planes about the fibre axis, as evidenced by electron diffraction, shows that such sites would be available. The proposition accords with previous findings [9, 14] on the crystallographic dependence of the reaction between aluminium and carbon, higher reactivity at the edge of the basal plane of carbon than on the basal plane being reported. Such a mechanism is plausible because carbon atoms at a basal plane edge have uncompensated electron bonds and, energetically, favour the process.

(b) Carbide formation is diffusion controlled and occurs by the dissociation of carbon atoms from the fibre and their diffusion into the aluminium matrix.

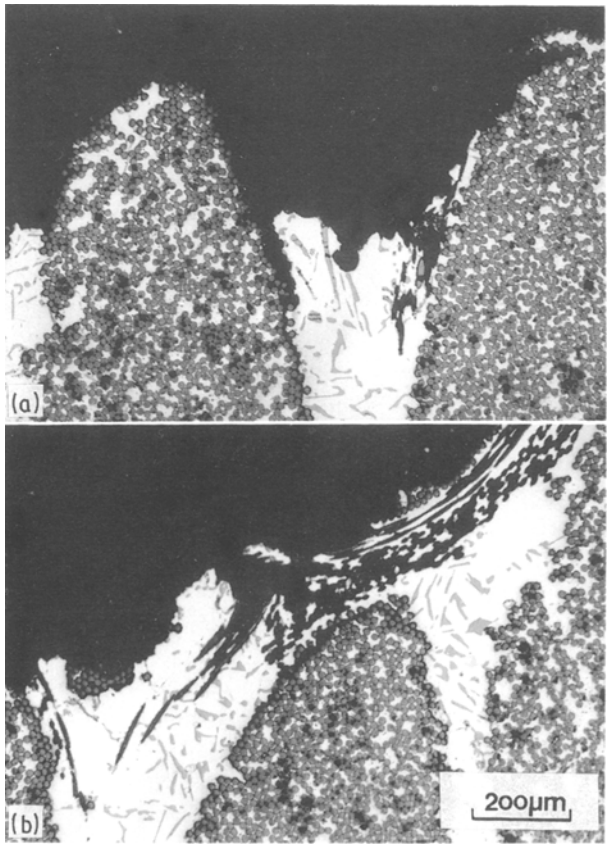

Figure 14 Tensile tested transverse specimen; polished section through fracture surface showing crack propagation along region of close fibre packing near edge of tow, OM.

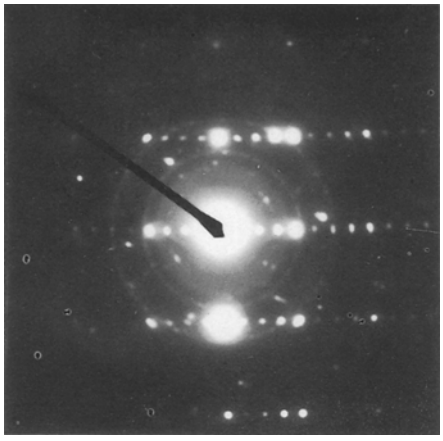

Figure 15 Electron diffraction pattern from fibre–aluminium interface after thermal treatment of composite for 24 h at 600 °C in argon; the spot pattern is due to Al_4C_3, the ring pattern to Al_2O_3.

(c) Growth of the carbide is highly anisotropic, being much faster in the [1 1 $\bar{2}$ 0] direction than in the [0 0 0 1] direction. This can be explained on the basis of the crystal symmetry of the aluminium carbide, which consists of hexagonal layers of aluminium atoms interspersed with layers of carbon atoms stacked in a regular sequence along the *c*-axis of the lattice [11]. These basal planes are closely packed and have a low surface energy. Hence carbon atoms diffusing through the matrix will migrate to the more favourable growth sites at the basal plane edge. Consequently, anisotropic growth of the carbide is expected, although it is not clear why the carbide assumes the shape of a lath rather than that of a platelet.

It has been argued that oxide is usually present at the fibre–matrix interface in an aluminium composite reinforced with carbon fibres. This was proposed by Everett *et al.* [10], who were able to distinguish between superficial oxide and interfacial oxide via the different binding energies revealed with a Rutherford backscattering spectrometer. In the present work, an electron diffraction pattern consisting of rings superimposed on spots (Fig. 15) was obtained from an interfacial region after thermal treatment of the composite at 600 °C for 24 h in an argon atmosphere. The spots were from aluminium carbide whilst the ring pattern could be indexed as gamma alumina. The crystalline nature of the alumina therefore suggests that it is present at the fibre–matrix interface since any superficial oxide would be present as the amorphous form.

4.2. Mechanical behaviour

The mechanical properties of the composite indicated that the potential of the material has by no means been realized. Using the rule of mixtures, the longitudinal strength of the composite is predicted to be 1.65 GPa, assuming a fibre volume fraction of 0.48, a fibre strength of 3.4 GPa and a matrix strength of 75 MPa. The experimentally measured value of ~ 300 MPa represents, therefore, only 18% of the calculated value, a very much smaller fibre contribution than reported by other workers. For example, Harris and Marsden [15] using chemical vapour deposition (CVD) and vacuum hot pressing methods to produce the composite, obtained a strength in the longitudinal direction close to that predicted by the rule of mixtures for a fibre volume fraction of 0.3 and showed that the reinforcing efficiency decreased as the volume fraction of the fibre increased. Similarly, Jackson *et al.* [16] observed in CVD and hot-pressed material that the strength was 75% of that predicted for 30% fibre and that it decreased markedly with increase in fibre volume fraction. It is perhaps, not surprising that published data vary so much as regards the efficiency of fibre reinforcement since not only is it dependent upon fibre type and volume fraction but also the fabrication process used to make the composite.

With the present composite several problems were identified, all of which were characteristics of the liquid metal infiltration technique used in its manufacture. Firstly, the pressure of the liquid metal had forced together fibres within individual tows, especially those situated near the edge of the tow. Their subsequent close packing, with many fibres actually touching one another, made it difficult to achieve effective infiltration and not surprisingly, some fibres were left with little or no matrix metal separating them. To this could be added the effect of the chemical reaction between fibre and matrix during processing. The aluminium carbide crystals which thus formed at the interface caused weakening of the fibre, as they drew upon it as a source of carbon, and also resulted in embrittlement of the surrounding metal matrix. Hence the problem caused by having only a restricted amount of metal present to separate individual fibres was compounded when some of this metal was converted to relatively brittle carbide. Indeed, it is not difficult to envisage a situation where the fibres in a bundle were separated almost entirely by carbide or by voidage, the net result in either case being the production of an almost completely embrittled region of composite. The silicon constituent in the matrix did not appear to alleviate matters. If anything the silicon platelets had the reverse effect by forming interfibre bridges and adding to the brittleness problem. Hence flaws, however they were initiated, spread rapidly across these regions to give the type of failure evidenced in the longitudinal specimen, Fig. 11a, that is catastrophic fracture of entire fibre bundles. Indeed, it appeared that a considerable volume of metal was needed in the path of the crack if there were to be any prospect of arresting its progress, Fig. 11b.

Fracture behaviour of the transverse specimen showed, by way of contrast, progressive breakage with a mixture of failure modes, including interfacial separation at edge of a tow, fibre splitting in the middle of a tow, as well as brittle fracture of glass fibres and localized plastic yielding of the matrix. The fibre splitting could have arisen because the fibre–matrix bond was stronger than the transverse strength of the carbon fibre.

Finally, it may be argued that some reduction in the volume fraction of fibre used in making the composite

might be beneficial in order to ensure that each fibre is (and remains) entirely surrounded by metal. The stress concentration which builds up at the tip of a crack may then be absorbed in the relatively ductile matrix regions, reducing the likelihood of an entire fibre bundle fracturing as if it were a single brittle constituent. The improvement in mechanical properties thence achieved might well outweigh any sacrifice made by reducing the fibre reinforcement potential.

5. Conclusions

The conclusions are as follows.

(a) Interaction between the carbon fibre and the aluminium constituent of the Al–Si alloy matrix occurred during fabrication which resulted in the formation of lath-like crystals at the fibre–matrix interface. The silicon constituent produced no such reaction with the fibre.

(b) The crystals consisted of rhombohedral aluminium carbide with the lath axis lying parallel to the basal plane of the carbide lattice.

(c) Carbide formation produced a strong fibre–matrix bond but reduced the fibre strength and embrittled the matrix. Thus in the longitudinal specimen, fibres failed at a low stress and cracks propagated through whole fibre bundles in a brittle manner to give catastrophic failure of the composite.

(d) The higher transverse strength may be attributed to a strong fibre–matrix bond coupled with the presence of the glass fibre weft.

Acknowledgements

We acknowledge the SERC and MOD for their support.

References

1. T. W. CHOU, A. KELLY and A. OKURA, *Composites* **16** (1985) 187.
2. R. L. TRUMPER, P. J. SHERWOOD and A. W. CLIFFORD, Materials in Aerospace, Proceedings of International Conference (Royal Aeronautical Society, London, 1986) p. 234.
3. N. MYKURA, International Symposium Cast Reinforced Metal Composites, edited by S. G. Fishman and A. K. Dhingra (ASM International, Pennsylvania, 1988) p. 173.
4. I. H. KHAN, *Met. Trans.* **7A** (1976) 1281.
5. S. J. BAKER and W. BONFIELD, *J. Mater. Sci.* **13** (1978) 1329.
6. A. OKURA and K. MOTOKI, *Comp. Sci. Technol.* **24** (1985) 243.
7. N. EUSTATHOPOLOUS, J. C. JOUD, P. DESRE and J. M. HICTER, *J. Mater. Sci.* **9** (1974) 1233.
8. T. OTANI, B. McENANEY and V. D. SCOTT, International Symposium Cast Reinforced Metal Composites, edited by S. G. Fishman and A. K. Dhingra (ASM International, Pennsylvania, 1988) p. 383.
9. L. F. MONDOLFO, "Aluminium Alloys, Structure and Properties" (Butterworths, London, 1976) p. 368.
10. EVERETT, W. HENSHAW, D. G. SIMSONS and D. J. LAND, "Composite Interfaces", edited by H. Ishida and J. L. Koenig (North-Holland, Amsterdam, 1986) p. 231.
11. G. A. JEFFERY and V. Y. WU, *Acta Crystallogr.* **20** (1966) 538.
12. "Smithells Metals Reference Book", 6 Edn edited by E. A. Brandes (Butterworths, London, 1983) pp. 8–23.
13. M. TAYA and R. J. ARSENAULT, "Metal Matrix Composites—Thermomechanical Behaviour" (Pergamon, Oxford, 1989) p. 247.
14. B. MARUYAMA and L. RABENBERG, "Interfaces in Metal Matrix Composites", edited by A. D. Dhingra and S. G. Fishman (ASM International, Pennsylvania, 1986) p. 233.
15. S. J. HARRIS and A. L. MARSDEN, "Practical Metallic Composites" (Institute of Metals, London, 1974) B35.
16. P. W. JACKSON, D. M. BRADDICK and P. J. WALKER, *Fibre Sci. Technol.* **5** (1972) 219.

Received 8 March
and accepted 15 March 1990